Nonlinear optical spectroscopy of indirect excitons in coupled quantum wells

P. Andreakou,[1] S. Cronenberger,[1] D. Scalbert,[1] A. Nalitov,[2] N. A. Gippius,[2,3] A. V. Kavokin,[4,5,6] M. Nawrocki,[7]
J. R. Leonard,[8] L. V. Butov,[8] K. L. Campman,[9] A. C. Gossard,[9] and M. Vladimirova[1]

[1]*Laboratoire Charles Coulomb, UMR 5221 CNRS/ Université de Montpellier, F-34095 Montpellier, France*

[2]*Institut Pascal, PHOTON-N2, Université Blaise Pascal, CNRS, 24 avenue des Landais, 63177 Aubière Cedex, France*

[3]*Skolkovo Institute of Science and Technology, Skolkovo, Moscow Region 143025, Russia*

[4]*Russian Quantum Center, 100, Novaya, Skolkovo, Moscow Region 143025, Russia*

[5]*School of Physics and Astronomy, University of Southampton, Southampton SO17 1BJ, United Kingdom*

[6]*Spin Optics Laboratory, St. Petersburg State University, 1, Ulianovskaya, St. Peterbsurg 198504, Russia*

[7]*Institute of Experimental Physics, University of Warsaw, Hoża 69, 00-681 Warsaw, Poland*

[8]*Department of Physics, University of California at San Diego, La Jolla, California 92093-0319, USA*

[9]*Materials Department, University of California at Santa Barbara, Santa Barbara, California 93106-5050, USA*

Indirect excitons in coupled quantum wells are long-living quasiparticles, explored in the studies of collective quantum states. We demonstrate that, despite the extremely low oscillator strength, their spin and population dynamics can by addressed by time-resolved pump-probe spectroscopy. Our experiments make it possible to unravel and compare spin dynamics of direct excitons, indirect excitons, and residual free electrons in coupled quantum wells. Measured spin relaxation time of indirect excitons exceeds not only one of direct excitons but also one of free electrons by two orders of magnitude.

I. INTRODUCTION

Indirect excitons (IXs)—bound pairs of spatially separated electrons and holes—form a model system to explore quantum properties of cold bosons in solids. Remarkable features of IX gases, including spontaneous coherence and condensation [1–3], long-range spin currents and spin textures [2,3], pattern formation [3–6], and correlation phenomena [7,8], have been recently demonstrated. The spin structure of IXs is particularly important. The exciton states with spin projections ±1 to the structure axis can couple to light to form bright states, while excitons with ±2 spin projections are dark. Typically, the dark states are lower in energy by electron-hole exchange interaction [9]. This basic property emphasizes the significance of the dark states and, in turn, of experimental techniques which can directly probe them. Nonlinear pump-probe spectroscopy can directly access the density and polarization state of both dark and bright components of the exciton gas, thus addressing one of great challenges in the exciton physics. The pump-probe spectroscopy has been successively applied to investigate electron [10], hole [11], direct exciton (DX) [12,13], and exciton-polariton [14] dynamics in nanostructures. But their application to IX spectroscopy is nontrivial because of the extremely low IX oscillator strength and has not been achieved until present.

In this article we report a proof-of-concept experiment demonstrating the potential of time-resolved pump-probe spectroscopy of IXs in coupled quantum wells (CQWs). The method is based on the three-level scheme [Fig. 1(a)]. In this scheme pump and probe light pulses are resonant with the optically active DX transition, and both bright and dark IXs are probed via their ground state, common with the DXs. The experiment reported here is the first realization of our theoretical proposal [15]. We show that both DX and IX spin and population dynamics, as well as the spin polarization of residual electrons, may be detected via the modulation of

reflectivity and Kerr rotation spectra at the DX resonances. From the photoinduced reflectivity measured as a function of the pump-probe delay we extract DX and IX radiative lifetimes varying from 1 to 30 ns, with a clear footprint of the gate-voltage-controlled DX-IX anticrossing. In the Kerr rotation signal, we unravel DX, IX, and electron spin dynamics. In unbiased CQWs electron spin contribution is negligible, and the coherent dynamics of DXs dominates. In biased CQWs the electron density and spin polarization build up. It appears that not only DX but also bare electron spin relaxation is much faster ($\simeq$200 ps) than the spin relaxation of IXs (up to 10 ns). We show that this is due to more efficient localization of IXs. From the spectral shape analysis of the nonlinear signals we conclude that the main mechanisms of the IX-DX interaction are the spin-independent narrowing of the DX resonance and the strongly spin-dependent blue shift of the DX energy.

II. SAMPLE AND EXPERIMENTAL SETUP

Our sample consists of two 8-nm-wide GaAs quantum wells separated by a 4-nm $Al_{0.33}Ga_{0.67}As$ barrier and surrounded by 200-nm $Al_{0.33}Ga_{0.67}As$ layers. The voltage V_g applied between the conducting n-GaAs layers drops in the insulating layer between them [16]. The sample is placed in the helium bath cryostat. We perform Kerr rotation and photoinduced reflectivity experiments at 2 K. Spin-polarized DXs are optically excited in the CQW by a circularly polarized pump pulse, Fig. 1. The resulting dynamics of the spin polarization (density) is monitored via Kerr rotation (reflectivity) of the delayed linearly polarized probe pulse. Two-color measurements are realized by spectral filtering of pump and probe pulses. The pulse duration is 1 ps, and the spectral width is 1.5 meV. The Ti-sapphire laser repetition rate is reduced to 20 MHz in order to avoid exciton accumulation between pulses. Typical powers
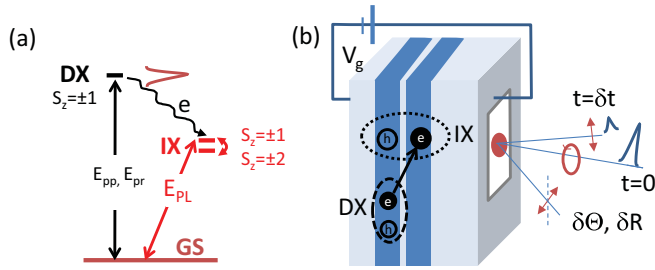
FIG. 1. (Color online) (a) Three-levels scheme of the pump-probe experiment with relevant excitonic states in a biased CQWs. Low-oscillator-strength IX states are pumped (E_{pp}) and probed (E_{pr}) via DX transition through their common ground state. (b) Sketch of CQWs and pump-probe experiment.

FIG. 3. (Color online) Reflectivity induced by pump pulses resonant with DX transition ($E_{pp} = 1.568$ eV), measured as a function of the pump-probe delay and probe energy at $V_g = 0$ (a) and $V_g = 0.8$ V (b).

are 120 and 70 μW for pump and probe, respectively, focused on the 100-μm-diameter spot.[1]

The exciton states in CQWs are formed from four possible electron-hole pair states in two individual QWs. The corresponding exciton energies and oscillator strengths can be accurately calculated by solving Schrödinger equations for different values of the gate voltage [17]. An example of such a calculation for our sample is given in Fig. 2(a), where a gray-scale map of the excitonic absorbtion in CQWs is shown on the energy/gate voltage plane. The resulting DX-IX anticrossing is well described by the simple two-level anticrossing picture. The excitonic energies obtained within the two coupled oscillators model are shown as colored lines in Fig. 2(a), and the oscillator strengths, which are inversely proportional to the exciton lifetimes, are shown in Fig. 2(b). At $V_g = 0$, DX is the ground state of the system, IX is only several meV above it, and its oscillator strength is only 10 times smaller. By contrast, at $V_g = 0.8$ V, the IX state is about 16 meV below the DX and has an oscillator strength 100 times smaller than DX. At intermediate gate voltages, an anticrossing between IX and DX states is expected. In this regime, the fastest recombination of IXs is expected in CQWs.

III. PHOTOINDUCED REFLECTIVITY

We address the dynamics of exciton population in CQWs at different gate voltages by probing dynamics of the photoinduced reflectivity signal δR. Figure 3 shows δR measured as a function of the pump-probe delay δt and probe energy E_{pr}, at fixed pump energy $E_{pp} = 1.568$ eV. These data show that even in the unbiased device the photoinduced reflectivity, and thus the exciton population, persists as long as 5 ns. At short pump-probe delays, a double resonance structure is apparent. In the biased structure the spectral profile of δR also changes significantly during the first nanosecond after the pump pulse. However, a strong signal persists at the longest delays studied. Decreasing the time interval between laser pulses from 48 to 24 ns leads to the accumulation of the excitons between pulses and the pump-probe signal at negative delays builds up. This means that the lifetime of excitons in this structure is of the order of 30 ns, consistent with the IX photoluminescence kinetics measurements [16].

Figure 4(a) shows typical time scans of the photoinduced reflectivity at three different values of the gate voltage and fixed probe energy. This nonmonotonous behavior is due to the shift of the spectrum during the first nanosecond after the pump pulse (Fig. 3). At longer delays the decay becomes biexponential, with the characteristic times plotted in Fig. 4(b) as a function of the gate voltage. While the shortest decay

---

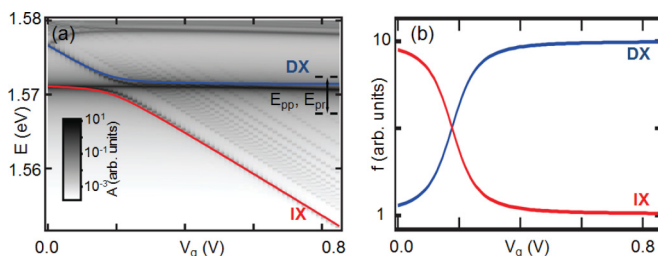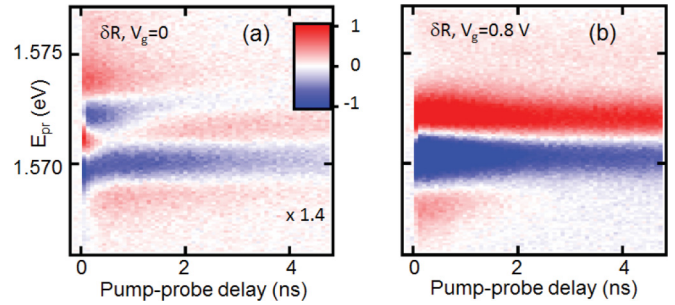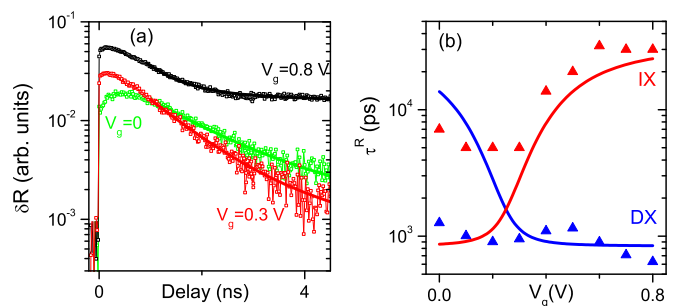[1]We have checked that reducing the probe-to-pump power ratio does not change the signal dynamics.

FIG. 2. (Color online) Oscillator strengths (a) and energies (b) of DX and IX calculated from the coupled oscillators model as a function of the gate voltage. Color map in (b) shows accurate solution for excitonic absorbtion.

FIG. 4. (Color online) (a) Photoinduced reflectivity measured (symbols) as a function of δt at $E_{pr} = 1.570$ eV, solid lines are fit to biexponential decay. Pump energy $E_{pp} = 1.568$ eV. (b) IX and DX lifetimes extracted from biexponential fit of the reflectivity decay (symbols), and inverse oscillator strengths of DX and IX coupled oscillators (lines).

time $\sim$1 ns does not depend on the voltage, the longer decay time has a pronounced voltage dependence. The decay of the excitonic population is faster at $V_g = 0.3$ V than the decay in the unbiased device.

The observed dynamics of the exciton population, as well as its voltage dependence, can be understood as a footprint of both DXs and IXs and their voltage-controlled anticrossing. The fast decay of the δR signal is due to DX recombination, and slow relaxation is due to IXs recombination [Fig. 4(b)]. Remarkably, neither pump nor probe pulses are resonant with IX transition, so the entire nonlinear signal results from DX-IX interaction. The complex spectral shape and dynamics of δR at short pump-probe delays is due to the high exciton density, and its detailed understanding is beyond the scope of this work.

IV. PHOTOINDUCED KERR ROTATION

Kerr rotation measurements provide the information on the spin dynamics in CQWs and the results are even more intriguing (Fig. 5). At $V_g = 0$ the rapid decay of $\delta\Theta$ is accompanied by the inversion of the derivative-like spectrum at 0.5 ns. In contrast, at $V_g = 0.8$ V the rapid decay is followed by much slower relaxation on the scale of several nanoseconds without the inversion of the spectrum. In Fig. 6(a) we plot the Kerr rotation measured at fixed probe energy. At $V_g = 0$ the signal is nonmonotonous, consistent with the spectrally resolved measurements of Fig. 5(a). At higher voltages, the decay is triple exponential, with the longest spin lifetime reaching 10 ns. The decay times obtained by fitting the data at different gate voltages are summarized in Fig. 6(b).

We propose the following interpretation of these observations. First, in semiconductor heterostructures a small splitting between two perpendicularly polarized linear exciton states δ_{xy} is generally present [2,18]. For an exciton spin this splitting acts as an effective in-plane magnetic field. Therefore, relaxation of the spin polarization is accompanied by its rotation around this effective field. Indeed, Kerr rotation at zero and small bias is well described by the damped cosine function (solid line), assuming the Gaussian distribution of precession frequencies centered at 0.15 GHz, with the standard deviation ± 0.04 GHz. Coherent rotation of the exciton spin is limited by the stability of the hole spin within
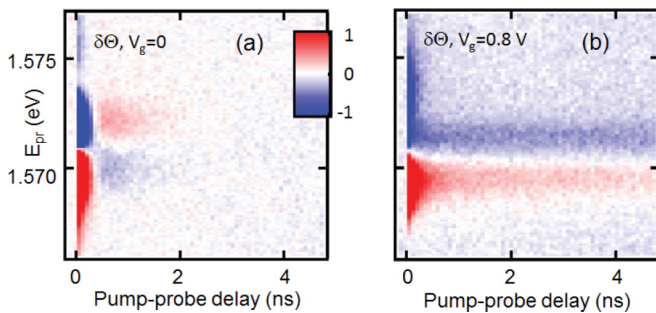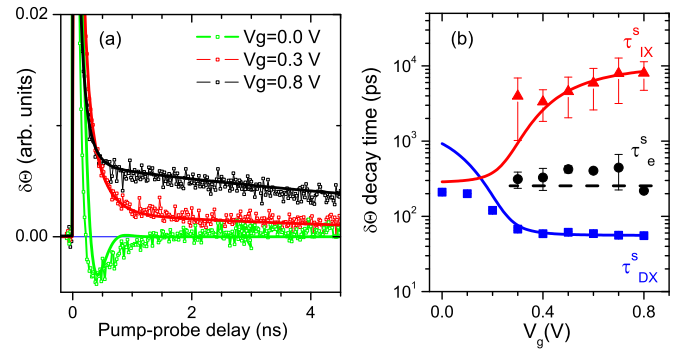

FIG. 6. (Color online) (a) Photoinduced Kerr rotation (symbols) as a function of δt at $E_{\mathrm{pr}} = 1.569$ eV, lines are damped cosine ($V_g = 0$) and triple exponential decay ($V_g = 0.3$ and 0.8 V) fitted curves. Pump energy $E_{\mathrm{pp}} = 1.568$ eV. (b) Spin lifetimes extracted from Kerr rotation decay as a function of gate voltage (symbols) and from the model (lines).

the exciton [19,20]. The hole spin relaxation time τ_s^h should satisfy $1/\tau_s^h < \delta_{\mathrm{exc}}/\hbar$, where δ_{exc} is the electron-hole exchange energy. Application of the electrical bias reduces the exchange energy [21], and the condition is no longer fulfilled. Indeed, at $V_g > 0.2$ V the Kerr rotation decay becomes monotonous. At high voltages, the shortest decay time of order of 50 ps can be attributed to the polarization relaxation of DXs [9,22]. The two other components have characteristic decay times of the order of 200 ps and several nanoseconds, respectively, the latter increasing with the gate voltage. They can be attributed to the spin relaxation of the 2DEG, which forms in biased CQWs [5,23,24] and IXs.

One of the main results of this work is the distinction between the spin-polarized IXs and the spin-polarized 2DEG traditionally studied by pump-probe Kerr rotation technique. The voltage dependence of the spin dynamics suggests that fastest and slowest components are due to DX and IX, respectively. We reproduce the voltage dependence of these two components within the model of the two coupled oscillators [lines in Fig. 6(b)]. By contrast, the electron spin relaxation is not expected to be strongly voltage dependent.[2] Within IXs we deal with the spin relaxation of an electron bound to the hole, but their exchange coupling is negligible at high V_g. The key parameter which controls the spin relaxation of electrons is the degree of their localization in the disorder potential [27]. Indeed, the electron spin relaxation time due to spin-orbit coupling can be written as $\tau_s^e = (1 + \tau_0/\tau_c)/(\tau_c\Omega_{\mathrm{SO}}^2)$ (see Appendix B). Here τ_0 is the characteristic time during which an electron remains localized and is not affected by the spin-orbit field, τ_c is the correlation time of the spin-orbit field,[3] and Ω_{SO}

FIG. 5. (Color online) Kerr rotation induced by pump pulses resonant with DX transition ($E_{\mathrm{pp}} = 1.568$ eV), measured as a function of the pump-probe delay and probe energy at $V_g = 0$ (a) and $V_g = 0.8$ V (b).

---

[2]The Rashba contribution to the spin-orbit field is small for this structure with respect to the Dresselhaus field [25,26]. In addition, the increasing Rashba field would affect in the similar way bare electrons and electrons bound into IXs.

[3]Correlation time of a fluctuating field is a time during which the field may be considered as constant. In the case of the spin-orbit field and mobile electrons it is given by the momentum scattering time, while in the hoping regime it is the time of flight.

is the spin-orbit frequency. Depending on the relative values of τ_c and τ_0, elections (IXs) are either localized ($\tau_c < \tau_0$) or mobile ($\tau_c < \tau_0$).

Faster spin relaxation is expected for mobile, than for localized electrons [27,28]. To check this idea, we studied the power dependence of the Kerr rotation. Increasing the pump power allows to increase the IX density up to the mobility threshold, while keeping the electron density fixed. The details on the exciton density dependence of the Kerr rotation signal are given in Appendix A. It turns out that the slow component disappears above a critical power. This corroborates the interpretation of the slow component in terms of the spin polarization of the localized IX. Increasing excitation power results to a gradual variation of the fast component that supports its assignment to the residual electron spin.

The ultimate test of this interpretation is the application of a longitudinal magnetic field, which suppresses spin relaxation of residual electrons much more efficiently than that of the electrons bound to holes within IXs. For electrons within IX the suppression factor is given by $\tau_s^{e,B}/\tau_s^e = 1 + (\Omega_L \tau_c)^2$, where Ω_L is the Larmor frequency [29]. For the electrons which are not bound into the excitons and thus are subject to the cyclotron motion, $\tau_s^{e,B}/\tau_s^e = 1 + (\Omega_c \tau_c)^2$, where Ω_c is the cyclotron frequency. Because the cyclotron frequency is usually higher than the Larmor frequency, spin relaxation of the free electrons is expected to be much strongly affected by the magnetic field.

Figure 7 shows Kerr rotation at $V_g = 0.8$ V as a function of the pump-probe delay at $B = 0$ and $B = 1$ T. Among the three decay components, only one with $\tau_s^e = 200$ ps is affected by the magnetic field. A systematic study of the magnetic field effect shows that it increases by a factor of 3 for all $V_g > 0.3$ V, as expected for the electrons, while the slow component remains unchanged, as expected for IXs. The analysis of these results in the framework of the spin-orbit relaxation model is reported in Appendix B. It allows for the identification of the fast decay as being due to the spin relaxation of resident electrons and the slow decay as being due to the localized IXs. The value $\tau_s^{IX} \sim 10$ ns is consistent with the polarization
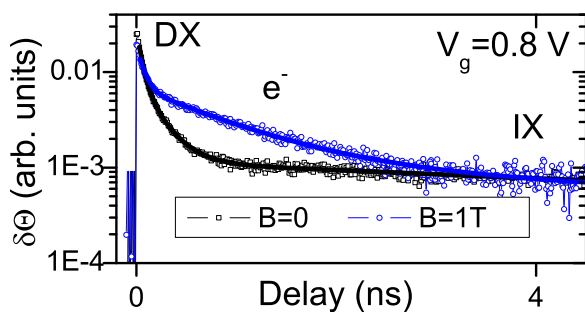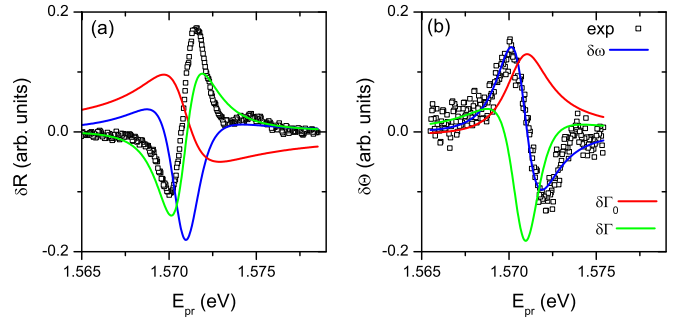

FIG. 8. (Color online) Probe spectra of photoinduced reflectivity (a) and Kerr rotation (b) measured at 5-ns pump-probe delay, $E_{pp} = 1.568$ nm (squares). Lines are calculated assuming photoinduced modification of the DX properties: energy blue shift (blue), saturation (red), and narrowing (green) [15].

lifetime of localized IXs measured in PL imaging experiments, corroborating our interpretation [30].

V. ORIGIN OF THE PUMP-PROBE SIGNAL

Spectral analysis of the δR and $\delta\Theta$ provide important information on the excitonic nonlinearities responsible for the buildup of the pump-probe signal. We focus here on the behavior at high voltages and long pump-probe delays, where the signal is dominated by IXs. Figure 8 shows the spectra measured at $V_g = 0.8$ V and $\delta t = 5$ ns. To identify the dominant nonlinearity we follow the roadmap proposed in Ref. [15]. First, we measure linear reflectivity in the vicinity of the DX resonance. The presence of IXs can modify the linear reflectivity via one of the three mechanisms: energy shift $\delta\omega$, saturation $\delta\Gamma_0$, and narrowing/broadening of the resonance $\delta\Gamma$ [15,31,32]. The spin-independent mechanisms contribute to the photoinduced reflectivity only, while spin-dependent ones are responsible for the Kerr rotation. Fitting to the data in Fig. 8(a) shows that the photoinduced reflectivity signal is dominated by the DX resonance narrowing. This can be understood as a reduction of the DX inhomogeneous broadening due to the screening of the QW disorder potential by localized IXs. Thus, at least at low IX densities, the impact of the DX blue shift due to the IX-DX interaction on the pump-probe spectra is weaker than that of the narrowing of the DX line. However, the blue shift of the DX resonance provides the main contribution to the Kerr rotation, Fig. 8(b). This is consistent with a strong spin dependence of the DX blue shift [15].

VI. CONCLUSION

In conclusion, we have shown that despite their vanishing oscillator strength, IXs in biased CQWs can be efficiently addressed by pump-probe spectroscopy. The detection of both photoinduced reflectivity and Kerr rotation provides a powerful tool for unraveling the spin dynamics of IXs and the 2DEG, exploring IX-DX interaction and probing both bright and dark IX populations. In appropriately chosen CQW devices, this method may help to solve the challenging problems of the exciton physics, which are not easily accessible by other

FIG. 7. (Color online) Photoinduced Kerr rotation (symbols) as a function of δt at $E_{pr} = 1.569$ eV without magnetic field (black squares) and at and under magnetic field $B = 1$ T applied in the growth direction (blue circles). Lines are triple exponential decay fit. IX spin decay is not affected by the magnetic field, while electron spin relaxation slows down.

experimental means, such as determination of relative density and spin polarization of the bright and dark IX states.

ACKNOWLEDGMENTS

APPENDIX A: DEPENDENCE OF THE INDIRECT EXCITON SPIN AND POPULATION ON THE PUMPING ENERGY AND POWER

In this section we show that at given pumping power, the spin polarization of indirect excitons (IX) is optimized for the excitation energy slightly below DX resonance and that this can be understood in terms of the density dependence of the exciton spin relaxation. Figure 9(a) shows Kerr rotation measured at $V_g = 0.8$ V for two different excitation energies and same power $P = 120\ \mu$W as the measurements shown in the main text. Probe energy is chosen to optimize the signal at 3-ns pump-probe delay. One can see that under high-energy pumping the slow component of the Kerr signal disappears completely, so no signal related to the IX spin dynamics can be identified. The energy of the pump beam with respect to the nonresonantly excited photoluminescence (PL) of the CQW device at the same gate voltage (black line) is shown in Fig. 9(b). One can see that the two pump energies are situated

FIG. 10. (Color online) Normalized Kerr rotation (blue) and photoinduced reflectivity (black) excitation spectra measured at $E_{pr} = 1.57$ eV and $V_g = 0.8$ V. Short pump-probe delay (5 ps, line) and long pump-probe delay (5 ns, symbols) are compared.

on the different sides of the DX emission line. For roughly a 1-meV shift between DX absorbtion and emission and 1.571 eV corresponding to the absorption maximum [24], we argue that at $E_{pp} = 1.571$ eV resonant excitation maximizes the IX density, while at $E_{pp} = 1.568$ eV the IX density is much lower. This is unambiguously confirmed by resonant PL experiments for this two pump energies [Fig. 9(b), green and red lines]. The PL measurements are taken in exactly the same conditions as the pump-probe measurements. For the high-energy excitation the IX emission is 3 meV above the IX emission at low energy excitation. The blue shift of the emission is a clear signature of the higher IX density n_{IX} and the resulting delocalization of IX, because the amplitude of the disorder potential is expected to be of order of 1 meV. In the framework of the plain capacitor model, the IX-IX interaction energy is given by $u_0 n_{IX}$, where $u_0 = 4\pi e^2 d/\epsilon$, d is the separation between the QWs, e is the electron charge, and ϵ is the background dielectric constant [33]. From the measured blue shift this approximation gives for the studied structure under high-energy excitation $n_{IX} \simeq 2 \times 10^{10}$ cm^{-2} and not more than 5×10^9 cm^{-2} at low energy excitation.

In order to confirm further the role of the exciton density in the spin relaxation processes, we report in Fig. 10 the normalized excitation spectra of the Kerr rotation and reflectivity measured immediately after the excitation (pump-probe delay $\delta t = 5$ ps) and at long delays $\delta t = 5$ ns. The probe energy was fixed at $E_{pr} = 1.57$ eV. One can see from the measurements at short delays that the same pumping energy optimizes the carrier density ($\propto \delta R$) and the spin density ($\propto \delta\Theta$) created by the pump pulse. By contrast, at $\delta t = 5$ ns the spin polarization is a trade-off between the initial polarization and the spin relaxation rate. The spin polarization maximum is achieved at lower energy than the maximum of the IX population.

Finally, it is important to check that decreasing the excitation power at $E_{pp} = 1.571$ eV allows us to recover the localization and slow spin relaxation of IXs. Figure 11 shows power dependence of the Kerr rotation signal at $V_g = 0.8$ V, $E_{pp} = 1.571$ eV, and solid lines are fits to bi- or three-exponential decay. With decreasing power, both electron and DX spin relaxation slow down progressively, but the slow component related to IX builds up only below the critical power (see inset of Fig. 11). This power should correspond to the IX density at which the IX-DX interaction energy is smaller than the disorder potential amplitude [7]. Thus we
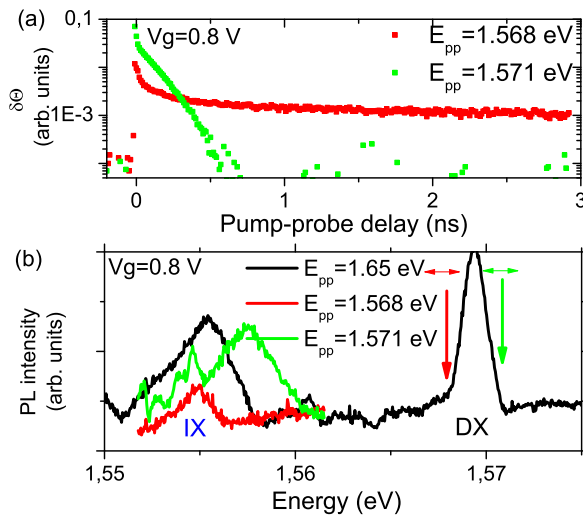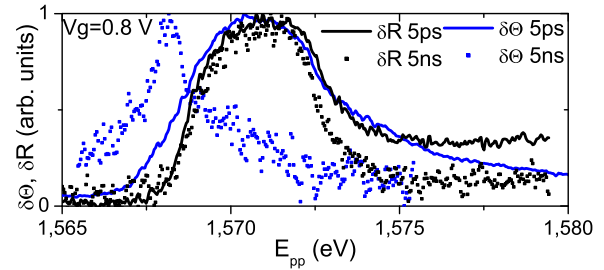

FIG. 9. (Color online) (a) Photoinduced Kerr rotation as a function of pump-probe delay measured at $E_{pr} = 1.569$ eV, $V_g = 0.8$ V. Pump energies are $E_{pp} = 1.568$ eV (red) and $E_{pp} = 1.571$ eV (green). (b) Photoluminescence spectra measured at $V_g = 0.8$ V for different excitation energies E_{pp}. IX emission is blue shifted at $E_{pp} = 1.571$ eV (green) with respect to $E_{pp} = 1.568$ eV (red) and nonresonant excitation $E_{pp} = 1.65$ eV (black).
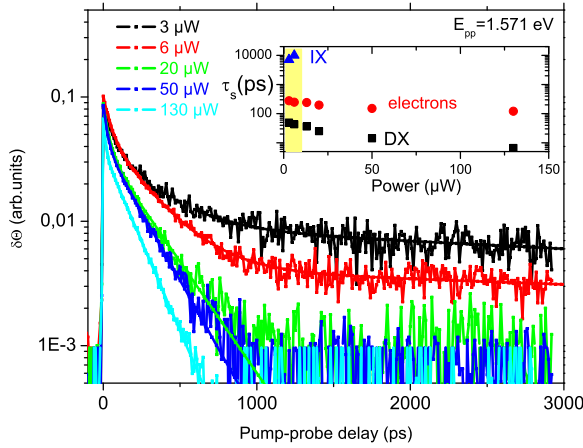
FIG. 11. (Color online) Kerr rotation (symbols) measured as a function of the pump-probe delay at $E_{pr} = 1.57$ eV, $V_g = 0.8$ V. At typical pump power $P_{pp} = 130$ μW used throughout this work no long-living spin polarization is detected at the pump energy $E_{pp} = 1.571$ eV. Decreasing the pump power allows us to recover the slow component. Solid lines are fits to biexponential ($P_{pp} = 130$ to $P_{pp} = 20$ μW) or tree-exponential ($P_{pp} = 6$ and $P_{pp} = 3$ μW) decay. Inset: Spin lifetimes of DXs, electrons, and IXs extracted from the fits. The spin lifetimes in the yellow region are similar to the results obtained at $E_{pp} = 1.568$ eV and $P_{pp} = 130$ μW, described in the main text.

conclude that IXs spin dynamics is mainly determined by its localization degree, Dyakonov-Perel spin relaxation being abruptly quenched for the excitation powers below IX localization transition.

APPENDIX B: MODEL FOR ELECTRON AND IX SPIN RELAXATION.

The key parameter which controls the spin relaxation of electrons is the degree of their localization in the disorder potential [27]. First, in the regime of the strongest localization the spin relaxation of electrons is due to hyperfine interaction with a limited number of nuclear spins, which acts on the electron as a fluctuating effective magnetic field. This type of relaxation is typical for electrons localized in natural quantum dots, the characteristic spin decay times are on the scale of nanoseconds, and this relaxation is efficiently suppressed by the longitudinal magnetic field of the order of mT [34,35]. In the experiments presented in this work, a long-living component of the spin polarization does not present any field dependence. Hence, we conclude that hyperfine field is not the main source of the spin relaxation in our CQWs and will neglect the spin relaxation of localized electrons (IXs).

The other source of relaxation is the fluctuating effective magnetic field due to spin-orbit interaction. While an electron (or IX) hops from one localization site to another, its spin experiences random rotations. In bulk zinc blende crystals this mechanism is a major cause of spin relaxation for the localized states in the impurity band [36]. In order to take into account the localization, we describe the diffusion of an electron (IX) in the QW in-plane disorder potential by 2 times. These are correlation times of the fluctuating spin-orbit field τ_c, during which the spin-orbit field can be considered as

constant, and τ_0, during which an electron remains localized and not affected by the spin-orbit field. The strength of the spin-orbit interaction is given by the root-mean-square value of the electron Larmor frequency in the spin-orbit field $\Omega_{SO} = 2\beta k/\hbar$, where $\beta = 2$ μeV μm is the spin-orbit constant [25,30] and k is the wave vector of the electron (IX). We shall assume that both residual electrons and electrons bound to holes within photoinduced IXs are characterized by their thermal wave vectors, $k_e = 17$ μm^{-1}, $k_{IX} = 10$ μm^{-1}, at $T = 2$ K. If the in-plane motion of an electron (IX) consist in hoping between the localization sites, the well-known Dyakonov-Perel formula for the spin relaxation time [29] should be scaled by the factor $1 + \tau_0/\tau_c$, so $\tau_s^{e(IX)} = (1 + \tau_0/\tau_c)/(\tau_c \Omega_{SO}^2)$.[4] In the limit of free carriers ($\tau_c \gg \tau_0$) this formula is reduced to the usual Dyakonov-Perel expression $\tau_s^{e(IX)} = 1/(\tau_c \Omega_{SO}^2)$. Note also that both τ_c and τ_0 depend on the carrier density and differ *a priori* for electrons and IXs in a CQW.

The longitudinal magnetic field affects differently the spins of residual electrons and the spins of electrons bound to holes within IXs. The precession of the electron spin in the longitudinal magnetic field averages out the random effective field due to spin-orbit interaction during the correlation time τ_c. The spin relaxation time in the presence of the magnetic field is given by $\tau_s^{e(IX)}(B) = (1 + (\Omega_L \tau_c)^2)\tau_s^{e(IX)}$, where Ω_L is the Larmor frequency [29]. For the electrons which are not bound into the excitons and thus are subject to the cyclotron motion, an additional mechanism further suppresses the Dyakonov-Perel relaxation [37]. In this case, the field induced increase of

---

[4]As the Dyakonov-Perel formula it is only valid in the limit of the slow angular diffusion $\Omega_{SO}\tau_c \ll 1$.
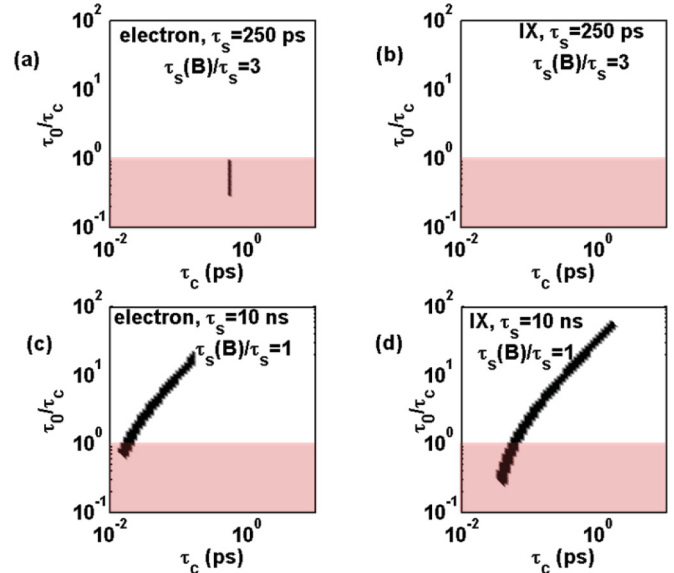

FIG. 12. (Color online) The two components of spin polarization signal mapped on (τ_c, τ_0/τ_c) parameter space. Pink areas denote the mobility area where $\tau_c > \tau_0$. The fast component ($\tau_s = 250$ ps, $\tau_s(B)/\tau_s = 3$) is calculated assuming either electron (a) or IX (b) spin relaxation. There are no points in the parameter space for the fast relaxation of IX. The slow component ($\tau_s = 10$ ns, $\tau_s(B)/\tau_s = 1$) can be obtained for both electrons (c) and excitons (d).

the spin relaxation time is given by $\tau_s^e(B) = [1 + (\Omega_c\tau_c)^2]\tau_s^e$, where Ω_c is the cyclotron frequency. Cyclotron frequency is two orders of magnitude higher than Larmor frequency so spin relaxation of the free electrons is expected to be much stronger affected by the magnetic field.

Our strategy is to map both experimentally observed spin components ($\tau_s = 250$ ps, $\tau_s(B)/\tau_s = 3$ and $\tau_s = 10$ ns, $\tau_s(B)/\tau_s = 1$) to this model. Figure 12 shows the result of such mapping for fast [Figs. 12(a) and 12(b)] and slow [Figs. 12(c) and 12(d)] components, assuming either electron [Figs. 12(a)

and 12(c)] or IX [Figs. 12(b) and 12(d)] relaxation. Pink areas mark the mobility region where $\tau_c > \tau_0$. Dark lines show the results of the calculation of the ratio τ_0/τ_c which fit the experimental results for each value of the correlation time. One can see that in Fig. 12(b) there are no dark points at all. This means that the fast component is necessarily due to electrons, mainly because it is strongly affected by the magnetic field. These electrons are mobile, since $\tau_c > \tau_0$. By exclusion, the slow component should result from the spin relaxation of IXs, which are essentially localized $\tau_c < \tau_0$.

[1] A. A. High, J. R. Leonard, A. T. Hammack, M. M. Fogler, L. V. Butov, A. V. Kavokin, K. L. Campman, and A. C. Gossard, Nature **483**, 584 (2012).

[2] A. A. High, A. T. Hammack, J. R. Leonard, S. Yang, L. V. Butov, T. Ostatnický, M. Vladimirova, A. V. Kavokin, T. C. H. Liew, K. L. Campman, and A. C. Gossard, Phys. Rev. Lett. **110**, 246403 (2013).

[3] M. Alloing, M. Beian, M. Lewenstein, D. Fuster, Y. González, L. González, R. Combescot, M. Combescot, and F. Dubin, Europhys. Lett. **107**, 10012 (2014).

[4] L. V. Butov, A. C. Gossard, and D. S. Chemla, Nature **418**, 751 (2002).

[5] L. V. Butov, L. S. Levitov, A. V. Mintsev, B. D. Simons, A. C. Gossard, and D. S. Chemla, Phys. Rev. Lett. **92**, 117404 (2004).

[6] M. Stern, V. Umansky, and I. Bar-Joseph, Science **343**, 55 (2014).

[7] M. Remeika, J. C. Graves, A. T. Hammack, A. D. Meyertholen, M. M. Fogler, L. V. Butov, M. Hanson, and A. C. Gossard, Phys. Rev. Lett. **102**, 186803 (2009).

[8] Y. Shilo, K. Cohen, B. Laikhtman, K. West, L. Pfeiffer, and R. Rapaport, Nat. Commun. **4**, 2325 (2013).

[9] M. Z. Maialle, E. A. de Andrada e Silva, and L. J. Sham, Phys. Rev. B **47**, 15776 (1993).

[10] J. M. Kikkawa, I. P. Smorchkova, N. Samarth, and D. D. Awschalom, Science **277**, 1284 (1997).

[11] M. Syperek, D. R. Yakovlev, A. Greilich, J. Misiewicz, M. Bayer, D. Reuter, and A. D. Wieck, Phys. Rev. Lett. **99**, 187401 (2007).

[12] M. T. Portella-Oberli, V. Ciulin, J. H. Berney, B. Deveaud, M. Kutrowski, and T. Wojtowicz, Phys. Rev. B **69**, 235311 (2004).

[13] A. Malinowski, R. S. Britton, T. Grevatt, R. T. Harley, D. A. Ritchie, and M. Y. Simmons, Phys. Rev. B **62**, 13034 (2000).

[14] A. Brunetti, M. Vladimirova, D. Scalbert, M. Nawrocki, A. V. Kavokin, I. A. Shelykh, and J. Bloch, Phys. Rev. B **74**, 241101 (2006).

[15] A. V. Nalitov, M. Vladimirova, A. V. Kavokin, L. V. Butov, and N. A. Gippius, Phys. Rev. B **89**, 155309 (2014).

[16] L. V. Butov, A. Imamoglu, A. V. Mintsev, K. L. Campman, and A. C. Gossard, Phys. Rev. B **59**, 1625 (1999).

[17] K. Sivalertporn, L. Mouchliadis, A. L. Ivanov, R. Philp, and E. A. Muljarov, Phys. Rev. B **85**, 045207 (2012).

[18] D. N. Krizhanovskii, D. Sanvitto, I. A. Shelykh, M. M. Glazov, G. Malpuech, D. D. Solnyshkov, A. Kavokin, S. Ceccarelli, M. S. Skolnick, and J. S. Roberts, Phys. Rev. B **73**, 073303 (2006).

[19] T. Amand, D. Robart, X. Marie, M. Brousseau, P. Le Jeune, and J. Barrau, Phys. Rev. B **55**, 9880 (1997).

[20] M. Dyakonov, X. Marie, T. Amand, P. Le Jeune, D. Robart, M. Brousseau, and J. Barrau, Phys. Rev. B **56**, 10412 (1997).

[21] G. Aichmayr, M. Jetter, L. Viña, J. Dickerson, F. Camino, and E. E. Mendez, Phys. Rev. Lett. **83**, 2433 (1999).

[22] T. C. Damen, K. Leo, J. Shah, and J. E. Cunningham, Appl. Phys. Lett. **58**, 1902 (1991).

[23] R. Rapaport, G. Chen, D. Snoke, S. H. Simon, L. Pfeiffer, K. West, Y. Liu, and S. Denev, Phys. Rev. Lett. **92**, 117405 (2004).

[24] L. Butov, A. Imamoglu, K. Campman, and A. Gossard, J. Exp. Theor. Phys. **92**, 260 (2001).

[25] K. Kavokin and M. Portnoi, Semiconductors **42**, 989 (2008).

[26] M. Studer, G. Salis, K. Ensslin, D. C. Driscoll, and A. C. Gossard, Phys. Rev. Lett. **103**, 027201 (2009).

[27] Z. Chen, S. G. Carter, R. Bratschitsch, P. Dawson, and S. T. Cundiff, Nat. Phys. **3**, 265 (2007).

[28] R. I. Dzhioev, K. V. Kavokin, V. L. Korenev, M. V. Lazarev, B. Y. Meltser, M. N. Stepanova, B. P. Zakharchenya, D. Gammon, and D. S. Katzer, Phys. Rev. B **66**, 245204 (2002).

[29] M. I. Dyakonov (ed.), *Spin Physics in Semiconductors*, Springer Series in Solid-State Sciences (Springer, Berlin, 2008).

[30] J. R. Leonard, Y. Y. Kuznetsova, S. Yang, L. V. Butov, T. Ostatnický, A. Kavokin, and A. C. Gossard, Nano Lett. **9**, 4204 (2009).

[31] L. V. Fokina, I. A. Yugova, D. R. Yakovlev, M. M. Glazov, I. A. Akimov, A. Greilich, D. Reuter, A. D. Wieck, and M. Bayer, Phys. Rev. B **81**, 195304 (2010).

[32] Z. Chen, S. G. Carter, R. Bratschitsch, and S. T. Cundiff, Physica E **42**, 1803 (2010).

[33] A. L. Ivanov, Europhys. Lett. **59**, 586 (2002).

[34] I. A. Merkulov, A. L. Efros, and M. Rosen, Phys. Rev. B **65**, 205309 (2002).

[35] I. Y. Gerlovin, Y. P. Efimov, Y. K. Dolgikh, S. A. Eliseev, V. V. Ovsyankin, V. V. Petrov, R. V. Cherbunin, I. V. Ignatiev, I. A. Yugova, L. V. Fokina, A. Greilich, D. R. Yakovlev, and M. Bayer, Phys. Rev. B **75**, 115330 (2007).

[36] K. V. Kavokin, Semicond. Sci. Technol. **23**, 114009 (2008).

[37] E. Ivchenko, Sov. Phys. Solid State **15**, 1048 (1976).